SANDIA REPORT

SAND2013-8329
Unlimited Release
Printed September, 2013

Thermal neutron detection using alkali halide scintillators with Li-6 and pulse shape discrimination

Erik Brubaker, Dean Dibble, Wondwosen Mengesha, Pin Yang

Prepared by
Sandia National Laboratories
Albuquerque, New Mexico 87185 and Livermore, California 94550

Sandia National Laboratories is a multi-program laboratory managed and operated by Sandia Corporation, a wholly owned subsidiary of Lockheed Martin Corporation, for the U.S. Department of Energy's National Nuclear Security Administration under contract DE-AC04-94AL85000.

Sandia National Laboratories

Issued by Sandia National Laboratories, operated for the United States Department of Energy by Sandia Corporation.

Available to DOE and DOE contractors from
U.S. Department of Energy
Office of Scientific and Technical Information
P.O. Box 62
Oak Ridge, TN 37831

Telephone: (865) 576-8401
Facsimile: (865) 576-5728
E-Mail: reports@adonis.osti.gov
Online ordering: http://www.osti.gov/bridge

Available to the public from
U.S. Department of Commerce
National Technical Information Service
5285 Port Royal Rd
Springfield, VA 22161

Telephone: (800) 553-6847
Facsimile: (703) 605-6900
E-Mail: orders@ntis.fedworld.gov
Online ordering: http://www.ntis.gov/help/ordermethods.asp?loc=7-4-0#online

SAND2013-8329
Unlimited Release
Printed September, 2013

Thermal neutron detection using alkali halide scintillators with Li-6 and pulse shape discrimination

Erik Brubaker Dean Dibble Wondwosen Mengesha Pin Yang

Abstract

An ideal ^{3}He detector replacement for the near- to medium-term future will use materials that are easy to produce and well understood, while maintaining thermal neutron detection efficiency and gamma rejection close to the ^{3}He standard. Toward this end, we investigated the use of standard alkali halide scintillators interfaced with ^{6}Li and read out with photomultiplier tubes (PMTs). Thermal neutrons are captured on ^{6}Li with high efficiency, emitting high-energy α and triton (^{3}H) reaction products. These particles deposit energy in the scintillator, providing a thermal neutron signal; discrimination against gamma interactions is possible via pulse shape discrimination (PSD), since heavy particles produce faster pulses in alkali halide crystals. We constructed and tested two classes of detectors based on this concept. In one case ^{6}Li is used as a dopant in polycrystalline NaI; in the other case a thin Li foil is used as a conversion layer. In the configurations studied here, these systems are sensitive to both gamma and neutron radiation, with discrimination between the two and good energy resolution for gamma spectroscopy. We present results from our investigations, including measurements of the neutron efficiency and gamma rejection for the two detector types. We also show a comparison with Cs_2LiYCl_6:Ce (CLYC), which is emerging as the standard scintillator for simultaneous gamma and thermal neutron detection, and also allows PSD. We conclude that ^{6}Li foil with CsI scintillating crystals has near-term promise as a thermal neutron detector in applications previously dominated by ^{3}He detectors. The other approach, ^{6}Li-doped alkali halides, has some potential, but require more work to understand material properties and improve fabrication processes.

Acknowledgment

This work was funded by DOE NNSA NA-22 Office of Non-proliferation Research and Development.

Contents

List of Figures

Chapter 1

Introduction

There are many ideas for thermal neutron detectors to replace ^{3}He, as necessitated by the global shortage of ^{3}He. Most if not all consist of one of the handful of other nuclei with high thermal neutron capture cross-sections, along with a medium sensitive to the products of that capture reaction. In the case that the capture agent is not the same as or part of the sensitive medium, the interface between them must be considered, and finally, for many applications a low sensitivity to gamma radiation must be maintained. For e.g. cargo screening and other homeland security applications, a level of 10^{-6}–10^{-7} is desired to successfully identify a neutron signal in the presence of the relatively higher expected gamma background flux.

Our proposed detectors use ^{6}Li as the capture agent, alkali halide crystalline scintillators as the sensitive medium, and PSD for gamma rejection; two ways of interfacing ^{6}Li with NaI or CsI are investigated. PSD in alkali halides is not commonly used in radiation detection, but has been studied [1, 2, 3]. Since the underlying sensitive medium has gamma sensitivity and good energy resolution, the resulting detectors are well suited for gamma spectroscopy as well as thermal neutron detection.

The goals of our investigation were to observe the anticipated thermal neutron signals and characterize the thermal neutron detection efficiency as a function of gamma background rejection. Rather than a full ROC curve analysis, we in fact measured the thermal neutron efficiency and gamma rejection at a single operating point. Feasibility was roughly defined at the outset as at least a 1% single-foil efficiency for the conversion layer approach, and at least a 5% efficiency in a 2" crystal for the doping approach; in each case with at most 10^{-4} gamma sensitivity.

We also performed to the extent possible identical measurements using a 25 mm dia. x 12 mm CLYC crystal from Hilger Crystals. CLYC is becoming widely used in the radiation detection community for thermal neutron detection, and like our approach can also provide gamma spectroscopy with medium energy resolution and pulse shape discrimination between gamma and neutron events [4, 5]. Good quality CLYC crystal growth is currently a challenge, especially in large sizes, resulting in high unit costs and limited crystal size. One advantage of using standard alkali halides interfaced with Li foil is low cost and good availability.

Chapter 2

Materials and Methods

Several prototype detector units were built for the studies described here. In general, due to the reactivity of lithium and hygroscopicity of alkali halide crystals, these detectors must be assembled in a controlled environment such as a dry box, and must be well sealed against air and moisture. Once a suitable container was developed, the assemblies were observed to be stable over one year, as efficiency measurements were repeated and results found to be consistent on that timescale.

Detectors based on lithium conversion layers

We interfaced a thin layer ($\approx$ 50 μm) of Li foil with NaI and CsI crystals, as seen in Fig. 2.1. For these studies, a single scintillating crystal was used, such that only one of the back-to-back reaction products can escape the foil into the crystal. A sandwich detector is also envisioned, where a coincident high-dE/dx event in two crystals would provide a highly specific thermal neutron signal. Most results shown here are from an assembly with a CsI(Tl) crystal, which was chosen partly for the simpler handling (lower hygroscopicity than NaI) and partly for its excellent PSD properties. For these feasibility studies we used natural lithium foil, with about 7% ^{6}Li abundance. Since ^{6}Li-enriched foil could be used to increase thermal neutron detection efficiency, we also report results extrapolated to that case for comparison to existing detection approaches.

Detectors based on lithium as a dopant

We also considered ^{6}Li as a dopant in NaI. Since lithium is also an alkali metal it is possible that Li could replace Na in the crystalline structure. We successfully formed a solid solution with $\approx$ 5% molar concentration of lithium, and produced polycrystalline NaI(Li,Tl) samples via hot pressing. The samples in their airtight housing are shown in Fig. 2.2. There is much room for refinement in the process, specifically to improve the transparency of the samples. As in Sec. 2, natural lithium raw materials were used to investigate feasibility, but using ^{6}Li-enriched salts would improve neutron detection efficiency.

Figure 2.1. Five tested detectors using Li foil interfaced with an alkali halide scintillator. Good hermetic sealing was needed to achieve stable detectors with no degradation of the Li foil.

Of course, LiI is itself a commonly used scintillator with thermal neutron sensitivity, typically Europium-activated [6]. Its primary disadvantages are low light yield, long scintillation decay time, and the absence of PSD to improve gamma rejection. The goal of this activity was to create a material with primarily NaI-like scintillation properties, but containing some Li for thermal neutron sensitivity.

CLYC detector

The CLYC detector used for comparisons was a 25 mm dia. x 12 mm right circular cylinder crystal acquired from Hilger Crystals, coupled with the same Hamamatsu H1949-50 PMT used for the other detectors. A standard bialkali photocathode is not ideal for the CLYC emission spectrum, so a potential improvement in light collection must be kept in mind. Our primary interest here is not the gamma energy resolution, but the PSD, where photostatistics enters as a secondary effect that can worsen the statistical separation between gamma and neutron events. The more important consideration was to be sure that the PMT timing, afterpulsing, etc., were consistent among the measurements. The crystal was mounted and sealed by Hilger in an aluminum can with window.

Figure 2.2. Polycrystalline NaI(Li,Tl) samples tested for thermal neutron sensitivity. Diverse color and transparency can be seen in these samples, indicating the sensitivity of the material to variations in the production process and dopant concentration.

^{3}He tube

As a reference detector, we used an LND model 253 ^{3}He tube. This tube has an effective volume of 364 cm^3 at a pressure of 4 atm. The signal from the tube was pre-amplified before feeding into an Ortec delay line amplifier. A baseline voltage was measured from the amplified output that was used to set a threshold. The amplified signal was fed into an Ortec 550A Single Channel Analyzer (SCA) and then into an Ortec counter. The SCA threshold was fixed at $\sim$ 200 mV. The tube sensitivity quoted by the manufacturer is 69.0 cps/nv.

Measurements

Each sample or detector assembly was wrapped in a diffuse reflector and hermetically sealed in a housing with plastic window, except the CLYC crystal, which was already similarly housed as described above. The unit to be tested was coupled with optical grease to a Hamamatsu H1949-50 PMT assembly. Pulse shapes were acquired with a Strück SIS3350 500 MS/s digitizer and written to disk for offline analysis.

Figure 2.3. A cave was constructed of HDPE and paraffin to moderate the fission spectrum neutrons emitted from ^{252}Cf and increase the flux of thermal neutrons through the detector.

Our neutron source was a sealed ^{252}Cf source. In order to increase the flux of thermal neutrons, we placed both source and detector inside a cave constructed of HDPE and paraffin to provide moderation of the neutrons (Fig. 2.3 and Fig. 2.4).

Offline analysis of the digitized pulses from the scintillator detectors proceeded as follows. First a baseline value was determined for each pulse using about 200 pre-trigger samples. If the RMS of the pre-trigger sample values was large, the baseline was considered unreliable and the pulse rejected. This step significantly improved the number of gamma pulses misreconstructed in the signal region of low PSD values. Pulse amplitude was calculated as the integral of the acquired pulse over baseline, while the pulse shape parameter corresponds to the number of samples (2 ns per sample) required to integrate from 10% to 80% of the area under the pulse. When necessary, the PSD algorithm was reoptimized due to the different time structure of the pulses from different detectors. We found that the rise time from 50% to 90% of the area under the pulse provided the best PSD separation for the NaI(Li,Tl) doped sample, and 1% to 10% for the CLYC crystal.

Figure 2.4. The ^{252}Cf source (cylinder with string attached) and the detector under test were placed in the center of the cave on an aluminum plate.

Chapter 3

Results

With the ^{3}He detector described in Sec. 2 along with the ^{252}Cf source inside the moderating cave, a count rate of 1070 Hz was observed. Using the listed tube sensitivity, this indicates a volumetric thermal neutron flux (nv) of 15.5 n/cm^2/s. A systematic uncertainty of 10% was assigned by considering variations in the measured flux with time and position of the source and detector within the cave.

Additional tests were performed with the ^{252}Cf source and the ^{3}He tube in different locations inside the HDPE/paraffin cave. Variations in the count rate on the order of 10% were observed. In Fig. 3.1, a comparison of ^{3}He count rate as a function of SCA threshold is shown for runs with and without an HDPE shielding block placed between the source and detector. The shape of the plot shows that our threshold selects neutron interactions including the triton and proton escape events (wall effect). The relatively small differences between the two runs implies that direct detection of fast neutrons from the ^{252}Cf source is not dominating the count rate.

Li-doped NaI

Results from a polycrystalline Li-doped NaI sample with a ^{252}Cf fission-spectrum neutron source in the moderating HDPE/paraffin cave are shown in Fig. 3.2. The scatter plot shows a pulse shape parameter vs. the pulse amplitude. The sample is only a few mm thick, which limits gamma efficiency and energy resolution, although thermal neutron efficiency is still expected to be relatively high due to a 5% molar concentration of Li. In addition, the sample transparency is also not ideal. Still, a thermal neutron signal can be identified as the population outlined by the green box, separated in pulse shape (y axis) from the more common gamma events. The thermal neutron detection rate is determined by counting the number of events in the signal region and dividing by the live time of the run. Over a 40 min run, a neutron detection rate of 0.5 Hz was observed.

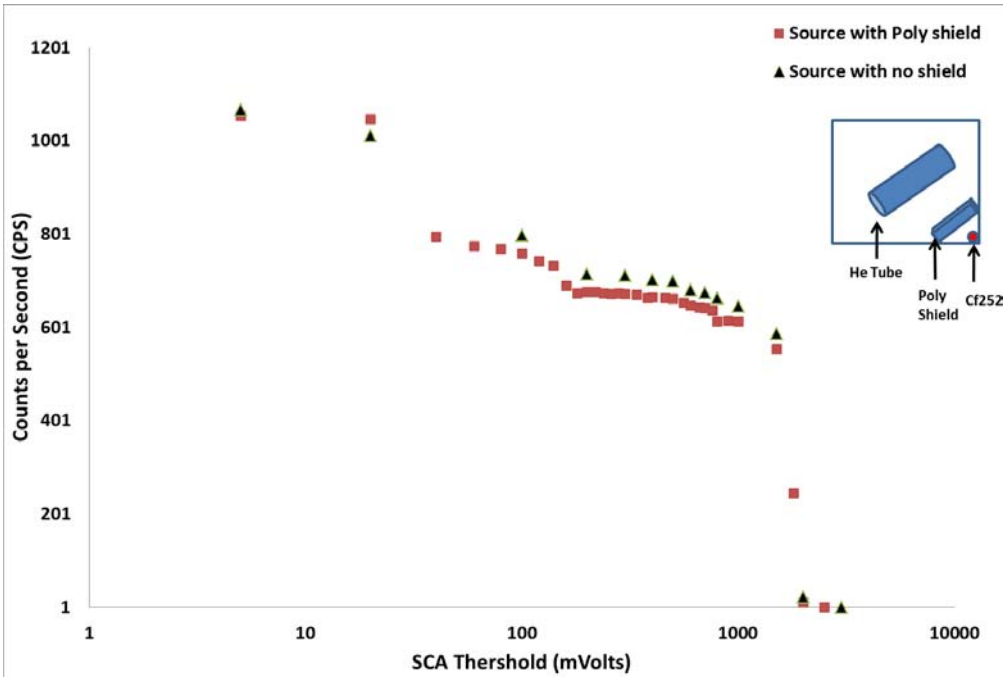

Figure 3.1. Count rate of the LND 253 ^{3}He tube as a function of threshold in mV. Similar rates are observed with and without a HDPE shielding block, indicating fast neutron detections are not dominant.

CsI(Tl) + Li foil

Results for the corresponding dataset using Li foil adjoined to CsI(Tl) are shown in a similar plot in Fig. 3.3. A clear signal, identified as an additional band in the scatter plot at lower PSD values, is observed in the presence of neutrons relative to the gamma-dominated background band. In fact, two populations of events can be resolved in the signal region. The α and ^{3}H reaction products are emitted back-to-back, so that from a given capture event, only one can escape the foil and be detected in the scintillator. The heavier α particle carries a lower fraction of the reaction Q value due to kinematic considerations, and its higher $\mathrm{d}E/\mathrm{d}X$ results in more energy quenching and a shorter pulse shape in the scintillator. Consequently, the α events are detected as a band at lower PSD values and with a lower amplitude endpoint. The longer, higher band corresponds to the triton detections, since ^{3}H starts with higher energy, experiences less quenching, and produces a wider pulse shape, all due to its lower mass and $\mathrm{d}E/\mathrm{d}X$.

The thermal neutron detection signal region is determined by eye, and is represented by a green box in Fig. 3.3. We count events in the signal region over a 24 hr run, and observe a neutron detection rate of 0.2 Hz. Since we used nat. Li foil, we also extrapolate the rate assuming 100% ^{6}Li enrichment. With enriched ^{6}Li foil, we would expect a detection rate of

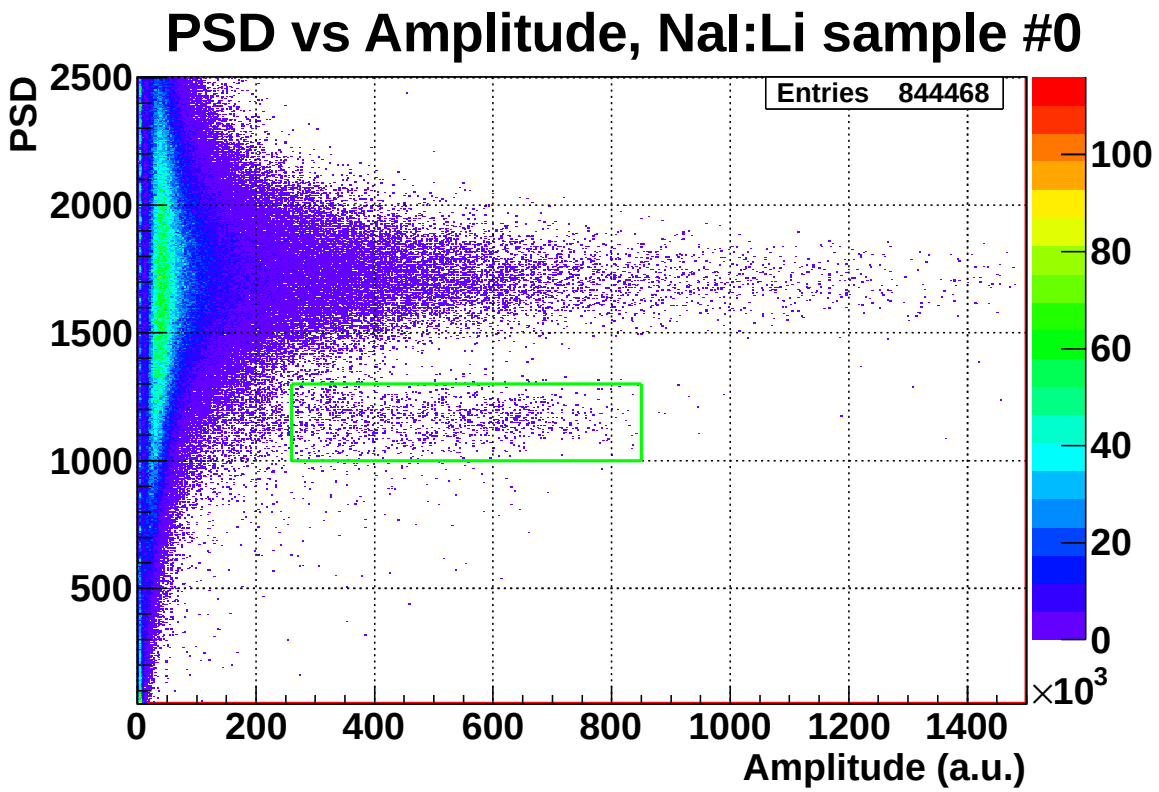

Figure 3.2. Pulse shape parameter vs pulse amplitude for polycrystalline Li-doped NaI in the presence of thermal neutrons. The band at 1700 in the pulse shape parameter corresponds to gamma events, while the band at 1200 corresponds to the triton and alpha recoils from thermal neutron capture on ^{6}Li embedded in the material.

2.5 Hz.

CLYC

A scatter plot of PSD vs pulse amplitude for the CLYC crystal inside the cave in the presence of thermal neutrons is shown in Fig. 3.4. There are several features of interest in this figure. Note the use of a log color scale to make low-intensity features more easily discernible. The high-intensity peak corresponds to thermal neutron capture events in which the α and triton recoils are fully contained. After quenching, the 4.8 MeV carried by the recoils results in about 3.2 MeV of electron-equivalent light output. The horizontal band at ~ 25 corresponds to gamma events. The horizontal band at ~ 50 likely consists primarily of fast neutron (n, p) interactions on ^{35}Cl [7], which occur at a high rate since the detector

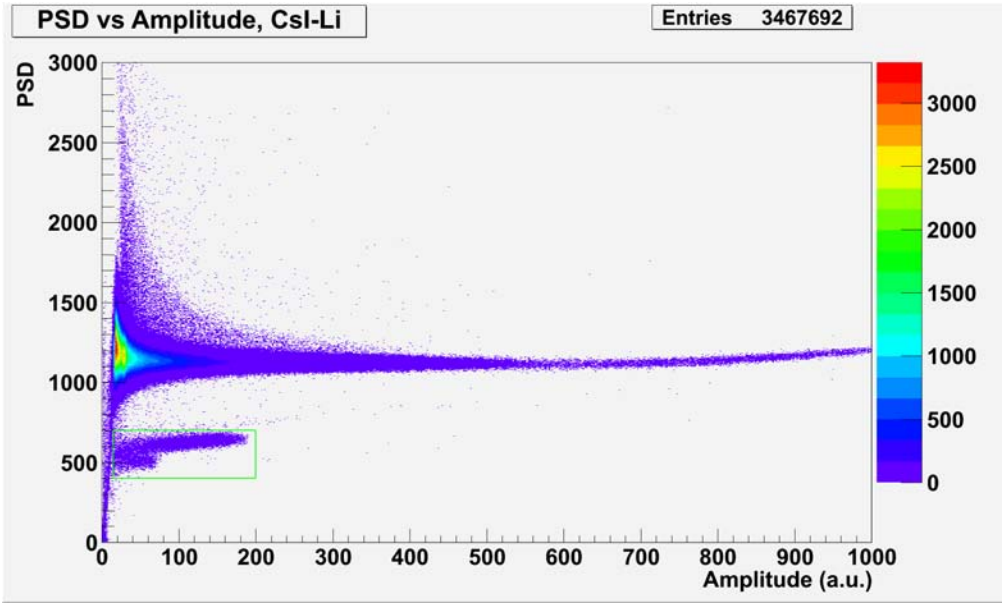

Figure 3.3. Pulse shape parameter vs pulse amplitude for a CsI(Tl) crystal adjoined to a thin Li foil in the presence of thermal neutrons. The band at $\sim$ 1100 in the pulse shape parameter corresponds to gamma events, while the two populations at 400–700 correspond to the triton and alpha recoils from thermal neutron capture on ^{6}Li in the foil.

is in very close proximity to the ^{252}Cf source. The ^{6}Li capture events can also be broadened horizontally, to lower amplitude by escaping reaction products, and to higher amplitude by fast neutron captures where the kinetic energy of the neutron is added to the α and triton energies.

As described above, we count neutron events in the signal region (purple box in Fig. 3.4), and divide by the live time to determine a thermal neutron detection rate. We also use the sidebands of the neutron amplitude distribution to fit and subtract the fast neutron contribution under the thermal capture peak. That correction is $O(1\%)$, and the correction to the detected neutron rate in the opposite direction for deadtime in the data acquisition is even smaller. Over roughly 24 hr of data collection, we observed a thermal neutron detection rate of 10.4 Hz. The CLYC crystal is already ^{6}Li enriched, so no extrapolation is needed in this case.

Gamma rejection

For the Li-doped NaI, the observed pulse shape separation is not sufficient for good gamma-neutron discrimination, though improvements may be possible with changes in the

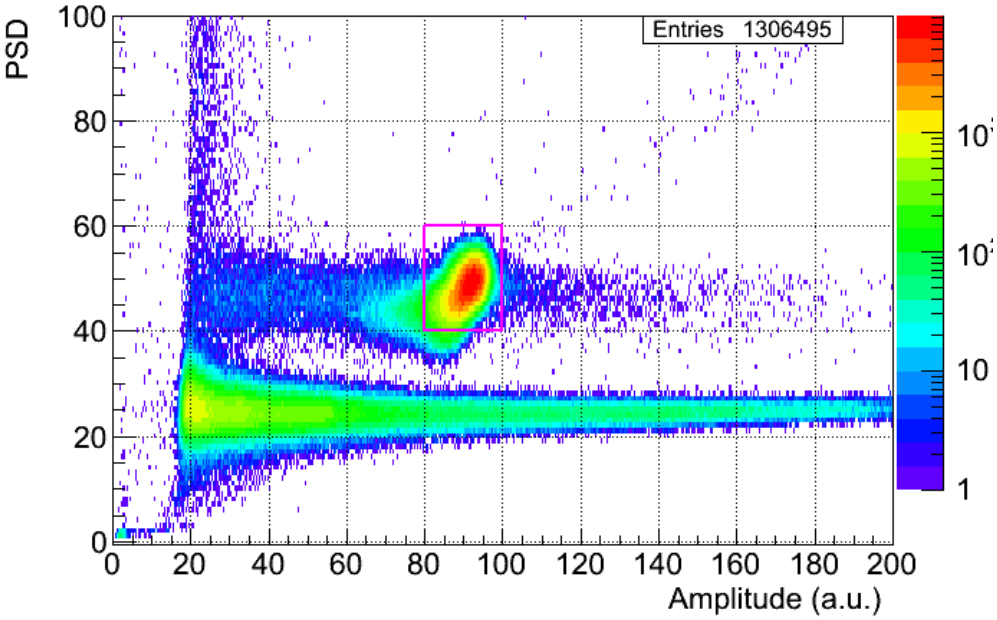

Figure 3.4. Scatter plot of the PSD parameter vs pulse amplitude for the CLYC crystal in the presence of thermal neutrons. A log color scale is used to better resolve the low-intensity features. The horizontal band at ~ 25 corresponds to gamma events, the large peak to thermal neutrons with full capture of the reaction products, and the rest of the horizontal band at ~ 50 to fast and thermal neutron events.

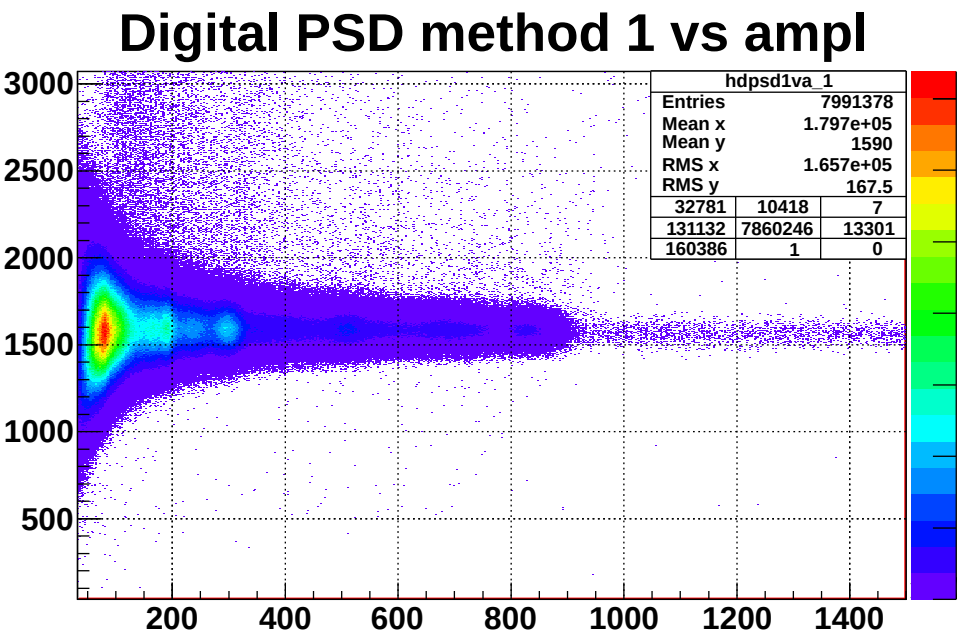

Figure 3.5. Pulse shape parameter vs pulse amplitude for a CsI(Tl) crystal adjoined to a thin Li foil in the presence of a strong gamma flux from ^{232}Th. Events falling within the signal region are used to measure an upper limit on the misidentification rate of gammas as thermal neutrons.

material preparation. For Li foil coupled to CsI the PSD separation is excellent, so a quantitative estimate of the gamma rejection was made. In the case of CLYC, gamma-neutron separation is also aided by pulse height discrimination, since the 3.2 MeVee observed energy for thermal capture events is higher than any naturally occuring gamma backgrounds.

The detectors were tested in the presence of a strong ^{232}Th source to evaluate the gamma rejection capabilities. Figure 3.5 shows the PSD vs amplitude plot for the CsI(Tl) crystal with Li foil conversion layer. Using the ratio of the number of events falling in the thermal neutron signal region[1] to the total number of events detected, we calculate an upper limit on the gamma sensitivity of this detector of 2×10^{-6}. Since there is a real thermal neutron background contributing to the detected signal events, and since not all gammas passing through the detector are registered and therefore included in the denominator, the real gamma sensitivity is likely closer to 2×10^{-7} for the gamma spectrum from this source.

In Fig. 3.6 the corresponding run is shown for the CLYC detector. No events are seen in the thermal neutron signal region (from Fig. 3.4), in large part due to the paucity of any

[1]Note that Fig. 3.5 and Fig. 3.3 used slightly different parameters for the PSD algorithm, resulting in a different PSD value for the gamma band. The signal region used for the gamma sensitivity analysis was appropriately chosen.

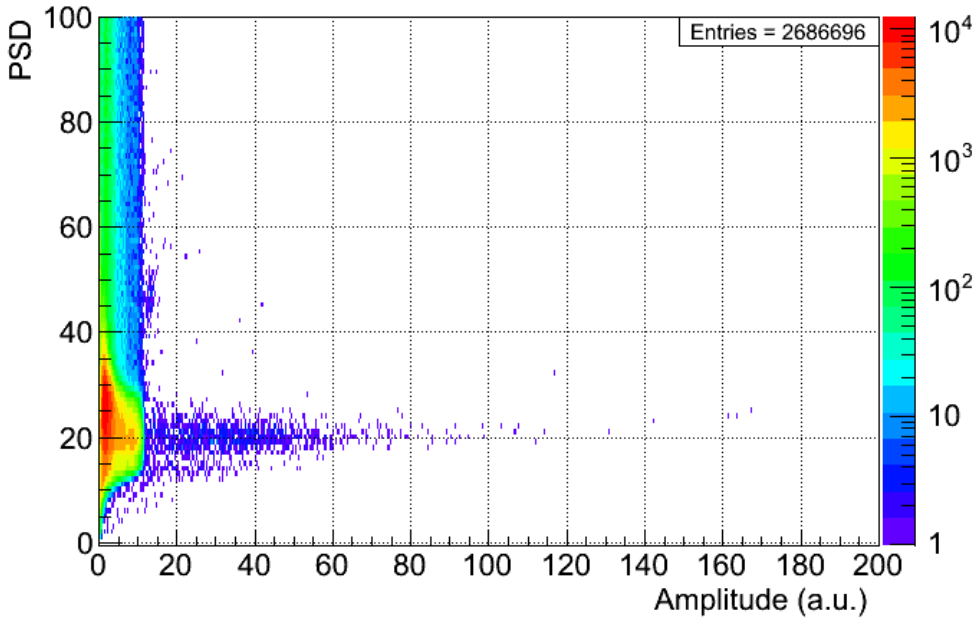

Figure 3.6. Pulse shape parameter vs pulse amplitude for a CLYC detector in the presence of a strong gamma flux from ^{232}Th. No events fall within the signal region outlined in Fig. 3.4.

gamma events at that amplitude.

Ideally, the probability of gamma misidentification would be measured as a function of amplitude so that a prediction for false neutron rate could be calculated for any gamma spectrum. That would be particularly difficult for CLYC as a pure gamma source covering the 2–5 MeV range would have to be used.

Table 4.1. Summary of the measurements.

Detector	Neutron rate (cps)	Surface area (cm^2)	Volume (cm^3)	Capture nuclei (est.)
^{3}He	1070	341	364	5×10^{22}
CsI(Tl) + Li foil (nat. Li)	0.20	10.1 (Li)	6.4 (CsI)	9×10^{19}
CsI(Tl) + Li foil (100% ^{6}Li extrap.)	2.5	10.1 (Li)	6.4 (CsI)	1.2×10^{21}
CLYC	10.4	19.2	6.4	7×10^{22}

Chapter 4

Discussion

Thermal neutron measurements summary

The source and cave remained consistent throughout all the measurements with the exception of the Li-doped NaI detector, which was performed at an earlier time. As a result, the count rates can be directly compared among the other detectors. Table 4.1 summarizes the results from measurements with the ^{252}Cf source inside the HDPE/paraffin cave.

Two important caveats remain. The first is that clearly the count rates are determined partly by the active detection volume, as well as by the number of thermal neutron capture nuclei (^{3}He, ^{6}Li) present. Table 4.1 gives the surface area and volume of each detector to ease comparisons, as well as an estimate of the number of capture nuclei. For the CsI(Tl) + Li foil detector, the given volume is for the CsI(Tl) crystal, not the Li foil, which is only 50 μm thick; but the given surface area is for the foil alone, and includes a factor of two to account for the possibility that neutrons enter the foil from either side.

The second caveat is that the detectors themselves modify the thermal neutron field by detecting (absorbing) neutrons. If the detector is efficient enough to become a significant thermal neutron sink, the count rate can saturate as it approaches the thermal neutron source rate. (Here the thermal neutron source is the system of ^{252}Cf source and HDPE/paraffin moderator.) Put another way, if the thermal neutron average flux contains contributions from the same neutron passing through the detection volume multiple times as it scatters

around the cave, then a detection event will reduce that particle's contribution to the neutron field, and therefore the overall neutron flux. This effect will tend to make efficiency differences between detectors appear smaller than they are. We did not perform simulations or calculations to determine whether this is a significant effect in these measurements.

Neutron detection efficiency and gamma rejection

Given the observation of a signal, the thermal neutron detection efficiency was measured by comparing the rate of events in the signal region to the total thermal neutron flux through the surface of the polycrystalline sample or foil, as determined by the independent measurement with a ^{3}He detector.

Using the CsI(Tl) + Li foil detector as an example, the total surface area of the crystal through which neutrons can enter is $A = 10.1$ cm^2. Using the volumetric (nv) thermal neutron flux of $\Phi_V = 15.5$ n/cm^2/s measured as described above, we derive the corresponding unidirectional flux through a flat surface, which is lower by a factor of four: $\Phi = 3.9$ n/cm^2/s.[1] Finally, we calculate the thermal neutron detection efficiency using the (corrected) detected neutron rate R_n:

$$\epsilon_n = \frac{R_n}{\Phi \cdot A} = 0.5\%. \tag{4.1}$$

Results are summarized in Table 4.2. The measured efficiency corresponds to natural lithium foil or dopant, but using lithium 100% enriched in ^{6}Li would immediately increase the efficiency. An extrapolation to enriched materials is given in the table as well. Relative uncertainties of ±20% (measured) and ±30% (extrapolated) are dominated by systematic uncertainties in the thermal neutron flux (10%), a correction for the bulk crystal sensitivity to fast neutrons (≈ 10%), and in the extrapolation itself (≈ 15%). The doped sample has high thermal neutron efficiency due to the high concentration of Li atoms, but at this time is limited by gamma rejection power, and by significant work needed to scale the material to larger sizes.

In each case, we exceeded the detection efficiency goal set at the beginning of the project. For the foil detectors, single-foil efficiency was measured to be ∼ 0.5%, giving an extrapolated ^{6}Li-enriched efficiency of ∼ 6.9%, compared to the goal of 1%. For the doped detector, the measured efficiency was 5.2%, giving an extrapolated ^{6}Li-enriched efficiency of 53%, to be compared with the goal of 5%. As a point of reference, ^{3}He detector efficiency for thermal neutron detection can be up to ∼ 50–60%, depending on gas pressure, threshold, etc.

[1] The derivation proceeds by assuming an isotropic distribution of thermal neutron velocities and integrating their contributions to a surface flux.

Table 4.2. Summary of the measured efficiency and gamma rejection.

	Thermal n efficiency		
Sample	Measured (nat. Li)	Extrapolated (100% ^{6}Li)	γ rejection (^{232}Th)
NaI(Tl):LiI(5%)	5.2%	53%	Insufficient
CsI(Tl) + Li foil	0.5%	6.9%	$2 \times 10^{-6} - 2 \times 10^{-7}$
CLYC	N/A	14%	$< 1 \times 10^{-7}$
Uncertainty	$\pm$20% (rel.)	$\pm$30% (rel.)	

Chapter 5

Conclusion

We have investigated two substantially different approaches to interfacing ^{6}Li with alkali halide scintillating crystals. In summary, alkali halide scintillators with ^{6}Li conversion layers may be useful in the near term as thermal neutron detectors for ^{3}He replacement. We demonstrated a thermal neutron detection efficiency of $\sim$ 0.5% with natural Li foil and CsI(Tl), and extrapolate a single-foil efficiency of $\sim$ 7%, close to the theoretical maximum limited by the range of the reaction products in the Li foil. CsI(Tl) crystals also show good gamma rejection via pulse shape discrimination, on the order of 10^{-6} to 10^{-7}. Alkali halide scintillators doped with ^{6}Li are an interesting system with potential, but need more investigation. These are new materials that require careful characterization, optimization of doping levels, and refinement of the production process.

Comparing the alkali halide thermal neutron detectors developed in this feasibility study, and the industry-standard scintillator for thermal neutron detection, CLYC, ^{6}Li-enriched CLYC had a factor of $\sim$ 50 higher thermal neutron sensitivity than our CsI(Tl) + nat. Li foil detector sample of similar size. Since 100% enriched Li foil could be used, we extrapolate to the expected sensitivity difference in that case of a factor of $\sim$ 4. CLYC also has better gamma rejection due to good pulse height separation as well as pulse shape discrimination. However, the high cost and crystal size limitations of CLYC may make our solution more attractive for some applications.

Both of the new detector concepts described here have the potential for simultaneous gamma spectroscopy and thermal neutron detection with high efficiency, good gamma energy resolution, and gamma/neutron discrimination.

References

[1] C.M. Bartle and R.C. Haight. Small inorganic scintillators as neutron detectors. *Nuclear Instruments and Methods in Physics Research Section A: Accelerators, Spectrometers, Detectors and Associated Equipment*, 422(1-3):54–58, February 1999.

[2] Shinzou Kubota, Fumio Shiraishi, and Yasukiyo Takami. Decay Curves of NaI(Tl) Scintillators with Different Tl + Concentrations under Excitation of Electrons, Alpha Particles and Fission Fragments. *Journal of the Physics Society Japan*, 68(1):291–297, 1999.

[3] M.M. Hamada, F.E. Costa, M.C.C. Pereira, and S. Kubota. Dependence of scintillation characteristics in the CsI(Tl) crystal on Tl/sup +/ concentrations under electron and alpha particles excitations. *IEEE Transactions on Nuclear Science*, 48(4):1148–1153, 2001.

[4] A. Bessiere, P. Dorenbos, C.W.E. van Eijk, K.W. Kramer, and H.U. Gudel. New thermal neutron scintillators: $Cs_2LiYCl_6 : Ce^{3+} and Cs_2LiYBr_6 : Ce^{3+}$. *IEEE Transactions on Nuclear Science*, 51(5):2970–2972, October 2004.

[5] Jarek Glodo, William M. Higgins, Edgar V. D. van Loef, and Kanai S. Shah. Scintillation Properties of 1 Inch Cs_2LiYCl_6:Ce Crystals. *IEEE Transactions on Nuclear Science*, 55(3):1206–1209, June 2008.

[6] Guntram Pausch and Juergen Stein. Application of ^{6}LiI(Eu) Scintillators With Photodiode Readout for Neutron Counting in Mixed Gamma-Neutron Fields. *IEEE Transactions on Nuclear Science*, 55(3):1413–1419, June 2008.

[7] Jarek Glodo, Urmila Shirwadkar, Rastgo Hawrami, Tobias Achtzehn, H. Robert Andrews, E. Ted H. Clifford, Harry Ing, Vitaly D. Kovaltchouk, Martin B. Smith, and Kanai S. Shah. Fast Neutron Detection With Cs_2LiYCl_6. *IEEE Transactions on Nuclear Science*, 60(2):864–870, April 2013.

DISTRIBUTION:

1	MS 0899	Technical Library, 8944 (electronic copy)
1	MS 0359	D. Chavez, LDRD Office, 1911

Sandia National Laboratories